Synthesis Of Mesoporous Silica (SBA-16) Nanoparticles Using Silica Extracted from Stem Rice Husk Ash and Its Application in Electrocatalytic Oxidation of Methanol

Dr. Manish Deshpande¹, Amal S. Al-Raboei², Rahul Dasarwar³, Rajesh Bhise⁴, Ameer M. Al-Talqi⁵

^{1*}Head and Research Supervisor, Dept. Of Physics and Material Science, Netaji Subhashchandra Bose Arts, Commerce and Science College, Nanded, MS India-431601

²Department of Physics, Faculty of Applied Sciences and Humanities, Amran University, Republic of Yemen ³Research Scholar, Dept. Of Physics and Material Science, Netaji Subhashchandra Bose Arts, Commerce and Science College, Nanded, MS India-431601.

⁴Research Scholar, Dept. Of Physics and Material Science, Netaji Subhashchandra Bose Arts, Commerce and Science College, Nanded, MS India-431601

⁵School of Physical Sciences, Swami Ramanand Teerth Marathwada University, Nanded 431606, MS, India along with Department of physics, Faculty of Applied Sciences and Humanities, Amran University, Republic of Yemen.

Abstract

Aim: The aim of this study is to synthesize mesoporous silica (Santa Barbara Amorphous-16) nanoparticles from silica obtained from rice husk ash and to use them in the electrocatalytic oxidation of methanol.

Methods: The electrochemical oxidation of CH3OH is facilitated using a novel catalyst that is based on transformed mesoporous silica Santa Barbara Amorphous-16. Using SiO2/F127/BuOH/HCl/H2O gel, mesoporous silica Santa Barbara Amorphous-16 nanoparticles are hydrothermally produced in an acidic environment. An eco-friendly and cost-effective source of silica, stem rice husk ash is used to make pure SiO2 powder. The synthetic SBA-16 is studied by using BET, SEM,X-ray, TEM, and FT-IRmethods. Dispersing the synthesized SBA-16 in a 0.1 Mole solution of NiCl modifies it with Ni(II). The combination of NiSBA-16 with carbon paste results in analtered carbon paste electrode. Research using cyclic voltammetry and chronoamperometry was conducted on a modified electrode to study the electrocatalytic oxidation of CH3OH.

Result:Using NiSBA 16CPE results in a much higher oxidation current as compared to nonmodified CPE, as shown by cyclic voltammetry. The catalytic active sites for methanol oxidation are generated by the incorporation of Ni2+ into the channels of SBA-16.

Conclusion: It was found that anodic oxidation current rises at NiSBA-16CPE surface and in CH3OH, whereas cathodic current reduces

Keywords: Mesoporous silica, Methanol, Nanoparticles, Stem rice husk ash, SBA-16,

1. Introduction

Fuel cells are recognized as a potential storage of energy. They provide extremely efficient and eco-friendly technologies for the conversion of energy. They function at low temperatures and immediately transform the energy from a chemical process into electricity [1,2]. CH3OH serves as fuel in fuel cells due to its straightforward functioning, as well as its advantages in transportation and storage relative to H2-based fuel cells. The "direct methanol fuel cell (DMFC)" often exhibits sluggish kinetics and elevated overpotential at the surfaces of most used electrodes. MSNs, extensively utilized as catalyst and drug carriers, have garnered attention due to their substantial pore sizes, area of surfaces, and elevated thermal stabilities, which facilitate the immobilization of functional groups within their mesopores to enhance catalytic efficacy and drug performance [3-5]. The highly organized mesopores of MSNs facilitate molecular transfer. The pore diameters of mesoporous materials may be adjusted and typically range from 2 to 50 nanometers. Mesoporous material has found widespread use since its inception in several scientific fields, such as sensing, energy storage, and catalysis. The consistent pore size distribution with broad long-range order and large surface area (approximately 1000 m²/g) of these materials have piqued the curiosity of material scientists. The Santa Barbara Amorphous (SBA) family of mesoporous silica nanoparticles (MSNs), developed and synthesized at the "University of California in Santa Barbara," has been extensively studied because to its highly organized mesopores and substantial surface areas [6-8].

Santa Barbara Amorphous nanoparticle number 16 has been regarded as an alternate Santa Barbara Amorphous. The 3D pore structure of the open channels derived from the highly organized mesopores of Santa Barbara Amorphous-16

enhance the efficacy of incorporation, functionalization, transport of active catalysts and chemicals and adsorption studies [9-12]. Prior research has shown that SBA16 may be used in several medicinal applications, including selective supports for enzyme immobilization, medication delivery, and protein adsorption. Ho et al. synthesized Santa Barbara Amorphous-16 using a soul–gel technique, then used a hydrothermal approach to integrate tin as catalyst supports for investigating catalytic activity in the alkylation of aromatics with C6H5CH2Cl [13]. Their synthesis approach used white powder of silicon dioxide as the initial Silicon dioxid raw material, obtained from Rice husk that was chemically pre-treated before calcination. A non-ionic surfactant called pluronic F127 was used as the surfactant that directs the pores, while butanol was used as the co-surfactant. The Santa Barbara Amorphous -16 mesoporous silica nanoparticles were identified by HR-TEM images [14,15].

The use of rice husk as a silicon source for the synthesis of mesoporous silica nanoparticles (MSNs) has attracted interest owing to its abundance as a byproduct of rice cultivation. Rice husk is a notable agricultural byproduct in nations that grow and export uncooked rice as a principal agricultural commodity. Food and Agriculture Organisation (FAO) indicates that rice output reached 712.5 million tons in 2014, with around 20 wt% of husks. Incineration lowers the bulk by 80%, resulting in about 28.5 million tonnes of rice husk ash (RHA), a by-product that has garnered significant scientific attention and is used as a mineral additive [16,17]. In comparison to other natural fiber plants like cotton,bamboo, and bagasse, Rice husk has the greatest concentration, mostly including around 90 wt% SiO2. Among all plant wastes, rice husk ash has the greatest silica content. Rice plants absorb orthosilicic acid from groundwater, which is then polymerized to create amorphous silica in the husks. Rice husk (RH) is the external covering of the rice kernel, including two interlocking parts. The husk is removed from the rice grain since it is inedible. The majority of the husk is incinerated in fields, resulting in environmental issues, however minor amounts are used as a low-grade fuel in brick kilns and for low-pressure steam production, among other applications. In the developed world, husk is used for power generation via steam production, and the resultant ash is employed as a value-added component in the manufacture of high-performance concrete. Agro-industrial waste is plentiful in China, with rice husks likely being one of the most significant contributors. It may therefore be readily transformed into a value-added component for use in concrete. A number of studies have been conducted to assess the viability of RHA. Xu et al., 2012 demonstrate that RHA may serve as an economical building material. It enhances the system's longevity and may be used to manufacture highperformance concrete. SEM tests indicate that RHA is a porous pozzolanic material characterized by a significant quantity of holes ranging from 1 to 10 µm in size[18].

Electrotechnics, environmental research, and catalysis are just a few of the fields that have made use of functionalized and metal-incorporated Santa Barbara Amorphous-16 [19-21]. Cubic mesoporous silica SBA-16, in contrast to its hexagonal counterpart SBA-15, has received less attention from researchers. This might be because it requires a more specific and controlled set of production conditions. According to Tsoncheva et al., the dispersion of iron nanoparticles, which is controlled by the pore size of the support, has a substantial impact on the selectivity of CH3OH breakdown in Fe-modified mesoporous materials [22]. Based on mesoporous silica templates, Shon et al. developed a solvent-free infiltration approach to produce mesoporous tin oxide (SnO2) materials. Mesoporous SnO2 materials mimic the morphologies of their silica-based predecessors to a remarkable degree [23]. The creation of mesoporous and microporous materials relies heavily on silica, which may be extracted from these plants. This research focuses on the synthesis of mesoporous silica (Santa Barbara Amorphous-16) nanoparticles using silica obtained from rice husk ash, and their use in the electrocatalytic oxidation of methanol. The increasing need for sustainable energy solutions necessitates the urgent development of efficient and eco-friendly electrocatalysts for energy conversion applications, including methanol fuel cells. Mesoporous silica, specifically SBA-16, provides a substantial surface area and adjustable pore architecture, making it an advantageous support medium for catalysts. Employing rice husk ash as a silica source adheres to green chemistry principles, fostering waste-to-resource methodologies. This research seeks to generate economical and sustainable mesoporous silica nanoparticles for methanol oxidation, therefore aiding the advancement of alternate energy sources in the area of electrochemical catalysis.

This study analyzes the synthesis of mesoporous silica nanoparticles, especially Santa Barbara Amorphous-16, using silica obtained from rice husk ash (RHA) as a sustainable resource. The objective is to use these nanoparticles in the electrocatalytic oxidation of methanol. Subsequent to the introduction, the paper examines the current literature on mesoporous silica materials, highlighting their structural characteristics, synthesis methodologies, and prospective uses in catalysis. The methodology section outlines the experimental procedures for synthesizing SBA-16 and the characterisation techniques used to evaluate the material's structural and textural attributes. The results section delineates the findings about the performance of nanoparticles in methanol oxidation, emphasizing critical metrics of electrocatalytic efficiency. The discussion reviews the results, examines implications for catalysis applications, and tackles the study's shortcomings. The report finishes with suggestions for future research, emphasizing the optimization of these mesoporous materials for improved catalytic applications, particularly in energy-related fields.

2. Research Methodology

2.1 Equipment and Reagents

Powder of silicon dioxide was obtained from stem rice husk ashusing the technique established by Kalapathy et al. [24]. Polytriblock copolymer, HCl, and C₄H₉OH were acquired from Sigma. Powder of graphite, CH₃OH, NiCl₂, and NaOH were acquired from Merck. "XRD patterns were obtained using a Bruker D8 X-ray diffractometer (Germany) using

copper K-alpha radiation. The FT-IR spectra was obtained at room temperature using an FT-IR spectrometer, within the region of 500 to 3500 cm⁻¹. The structural and surface morphological analyses of the calcined mesoporous silica samples were conducted using scanning electron microscopy and TEM. X-ray fluorescence was used to assess the chemical composition of extracted powder of silica in oxide forms. The linear segment of the Brunauer-Emmett-Teller (BET) plots was used to ascertain the surface areas of the samples using BELSORP mini 100 equipment. The size of pore distribution was determined from N2 adsorption data using the traditional Barrett-Joyner-Halenda technique. Electrochemical investigations were conducted using the Dropsens bipotentiostat/galvanostat."

2.2 Silica powder is made from rice husk ash stems.

A black ash powder was originally produced by completely burning stem rice husk ash in air. White ash was obtained by calcining the black ash powder in an air atmosphere heated to 700 degree celsius. The ash powder, which contains silica, was mixed with 2 M NaOH while being vigorously stirred at 100 degree celsius for four hoursCrystalline metasilicic acid was obtained by filtering the solution, allowing it to cool to ambient temperature, and then neutralizing it with 1 mole of hydrochloric acid. A neutral medium was used to polycondensate the obtained silicic acid crystals for a duration of 18 hours. After being crushed in the beakers, it was rinsed with deionizedH2O to eliminate soluble salts. Overnight washing and drying at 70degreesCelsius yielded "pure silica xerogel". The mortar was used to grind Xerogel into a powder of pure silica. Scheme 1 depicts the several steps involved in making silica powder. Purified silica gel production is detailed in Eqs. (1) through (3):

SiO2 + 2NaOH → Na2SiO3 + H2O	1
Na2SiO3 + 2HC → 2NaCl + H2SiO3	2
$nH2SiO3 \rightarrow (SiO2)n + nH2O$	3
2.3 Nanoparticles using Mesoporous SBA-16 Synthe	sis

The structure-directing agent F127 was used in the hydrothermal synthesis of SBA-16. As a natural predecessor to silica, ash from rice husks was used to produce a powder of pure SiO2. Following standard synthetic procedures, a transparent gel solution was created by dissolving one gram of pure silica powder in eleven milliliters of 2.6 moles of NaOH. Then, along with 34 millilter of H2O and 2.8 mL of butanol, 0.7 gram of F127 was dissolved to make a solution. The solution was then slowly added 2.8 milliliters of 11.8 mol hydrochloric acid while being gently swirled for a whole day in order to produce a gel. Next, the gel was autoclaved with Teflon and heated in an oven at 100 degree celsius for

day in order to produce a gel. Next, the gel was autoclaved with Teflon and heated in an oven at 100 degree celsius for 24 hours. The gel was filtered, washed, and dried to complete the synthesis of mesoporous silica SBA-16. After six hours of calcination in air at 550 degree celsius, the organic template was removed.

2.4 Characterization of SBA-16

Stem rice husk ash is mostly composed of Silicon dioxide, with smaller amounts of Fe2O3,Na2O, Al2O3, MgO, K2O, and P2O5 also present. The chemical compositions of RHA as determined by XRF. A high amount of silica is indicated by this in stem rice husk ash. This work directly synthesized mesoporous silicon (SBA-16) using SCA as a silica precursor. The presence of a distinct diffraction peak at 0.84 (2q) and the Bragg reflection indicate that high crystallinity SBA16 has been synthesized. A noticeable band at 3500 centimeter per second is attributed to the stretching vibration of OeH bonds between silanol groups and adsorbed water molecules, whereas the band at 1646 cm⁻¹ is a result of the bending vibration mode. The main cause of the wide absorbance band between 1000 and 1300 cm⁻¹ is the presence of asymmetric stretching (AS) modes in the silicon dioxide vibrational module. "The in-phase motion of two neighboring O2 atoms in relation to the central silicon atom (AS1) and the out-of-phase motion of the identical O2 atoms in relation to the central silicon atom (AS2) are the two primary components of this band. Also, at around 960 cm⁻¹, the Si-OH group shows a bending vibration".

In SBA-16, the silicon oxide symmetric stretching modes are responsible for the presence of a band at 800-802 per centimeter. A band at 490 per centimeter stands out more, which is thought to be caused by the vibration of Si-O-Si bonds. Results from scanning electron microscopy and TEM analysis of the synthetic SBA-16 show that spherical SBA-16 nanoparticles ranging in size from 30 to 60 nm aggregate together. Additionally, there are high-quality, three-dimensional channels that go through the pores. An isotherm of type IV and a hysteresis loop of type H2 are features of the sample. The mesopores undergo capillary condensation of nitrogen at a pressure of P/P0 = 0.47.

Table 1 The XRF analysis of the stem rice husk revealed its chemical of weight percentage.								
Na2O	Al2O3	P2O5	Fe2O3	K2O	MgO	CaO	SiO2	
0.221	0.53	8.263	0.411	2.078	1.403	0.846	85.42	

2.5 Electrode preparation

Catalytically active mesoporous silica is created by substituting electroactive transition metal ions, such nickel(II) ions, for the cations, usually Na⁺, in the original material. The first stage in creating Ni(II) integrated SBA-16 was vigorously swirling a mixture of 10 milliliters of 0.1 M NiCl2 with 0.3 gram of SBA-16 24 hours after grinding. After that, the study centrifuged the sample to separate its components, rinsed it with deionized water to get rid of any residual Cl ions, and then dried it in the oven for the night. A modified carbon paste electrode with a 30 percent (w/w) content was created by hand-blending 0.3 gram of NiSBA-16 with 0.7 gram of graphite powder in (C2H5)2O. Following the evaporation of the solvent, paraffin was added to make the paste. The finished product was placed in a 1.5 mm inner radius glass tube. An electrical connection was made using a copper wire. For 5 minutes, the modified electrode was

submerged in a solution of 0.1 Mole NiCl2. Control studies were conducted at CPE and NiCPE to better investigate NiSBA-16CPE's electrocatalytic properties in methanol oxidation.

3. Result

3.1 Effects of NiSBA-16CPE on Electrochemical reactions

Figure 1c illustrates the findings of the cyclic voltammetric analysis for NiSBA-16CPE in a 0.1 Mole NaOH solution, using a potential sweep rate of 25 megavolt per sec. The picture illustrates two separate redox peaks on the NiSBA-16CPE surface, signifying active electrochemical action. In the presence of methanol, the surface current of NiSBA-16CPE markedly increased, but the current for the unmodified carbon paste electrode (CPE) exhibited no variation, underscoring the electrocatalytic characteristics conferred by the Ni(II) alteration. The rise in current at the modified electrode is ascribed to the nickel active sites on the NiSBA-16CPE surface, which promote redox activity in an alkaline environment. Additionally, in the alkaline NaOH solution, mesoporous SBA-16 may experience ion exchange, whereby Ni²⁺ ions inside the structure may be substituted by Na⁺ ions from the solution. The exchange process may modify the stability and activity of the Ni(II) species on the electrode surface, thereby impacting the electrode's catalytic effectiveness over time. The existence of mesoporous channels in SBA-16 presumably facilitates methanol access to the catalytic sites, hence augmenting the total current response. These results illustrate the essential function of Ni(II) active sites within the mesoporous structure in facilitating methanol oxidation, potentially influencing the design of electrodes for energy conversion applications. Additional investigation into ion exchange effects and the optimization of Ni content in SBA-16 may boost catalytic performance and stability in fuel cell applications.

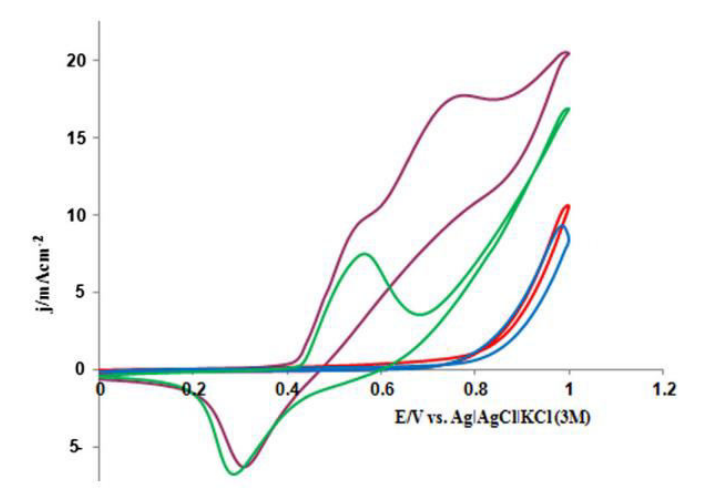


Figure 1. Cyclic voltammograms of CPE and NiSBA-16CPE at a rate of 25 mV sL1 in the presence of 0.03 M methanol in 0.1 M NaOH (b and d) and without (a and c) of this solution, respectively

The following is an illustration of the Ni2+–Na+ exchange at NiSBA-16CPE based on the mechanism suggested by Bessel and Rolison [20].

$$Ni_{(ms)}^{2+} + 2Na^+ \rightarrow Ni_{(int)}^{2+} + 2Na_{(ms)}^+$$
.....4

where ms (mesoporous silica), s (solution), and int (mesoporous silicaesolution interface) are appropriate descriptors. The redox process is carried out at the interface between NiSBA-16CPE and the electrolyte, where Ni2+ ions react with OH- to create nickel(II) hydroxide, as described in Reaction (5).

The following reaction occurs when "nickel(II) hydroxide oxidized to nickel oxyhydroxide during the anodic sweep, and when nickel oxyhydroxide is reduced to nickel(II) hydroxide in the cathodic direction" [25,26]:

$$Ni(OH)_2 + 2OH^- \rightarrow NiOOH + H_2O + e^-$$
.....6

At different scan speeds, the electrochemical behavior of "NiSBA-16CPE" studied in 0.1 Mole NaOH. At a scan rate of 15 mV per second, two redox peaks were seen, as shown in Figure 2A, with an E1/2 value of 421 mV and a DEp value of 152.5 mV. A rise in Δ Ep with the scan rate demonstrated a progressive charge transfer mechanism in the contacts between the electrolyte ions and the changed film. To use the formulae for peak-to-peak separation, one has to ensure that Δ Ep is more than 0.2/n Volt, where n is the number of electrons exchanged [27].

According to cyclic voltammograms taken of "NiSBA-16CPE in 0.1 M NaOH", the logarithm of the scan rate (n) affects both the cathodic and anodic peak potentials (Ep), which vary between 0.005 and 0.6 V per second. When the scan rate is more than 0.075 V per second, Laviron proved that Ep is proportional to log n. The electron transfer coefficients for the anodic (α) and cathodic (β) sites are 0.74 and 0.26, respectively, as shown in Figure 2B and computed using Equations (7) and (9). Evidence like this suggests that there could be separate rate-limiting phases in the anodic and cathodic processes [28]. With a scan rate of 300 mV per second, the average value of the standard rate constant (ks) is determined to be 0.064 per second. Also, the peak currents at the anode and cathode are precisely proportional to the scan rate with scan rates ranging from 0.005 to 0.075 Volt per second [29]. An equation representing a reversible process involving adsorbed species may be obtained from the linear part of the Iey diagram and used to calculate the surface coverage.

$$I_p = \frac{n^2 F^2 A \nu \Gamma^*}{4RT}.....10$$

"Ip signifies the peak current, A indicates the electrode surface area, and G defines the surface coverage of the redox species. The average of the cathodic and anodic currents indicates that the overall surface coverage of the immobilized active species is about 3.2×10^{-8} mol centimeter per square". At scan rates beyond 0.075 V per second, the anodic and cathodic peak currents are influenced by the square root of the scan rate (v¹/²), signifying that a diffusion-controlled mechanism progressively prevails with the elevation of the scan rate.

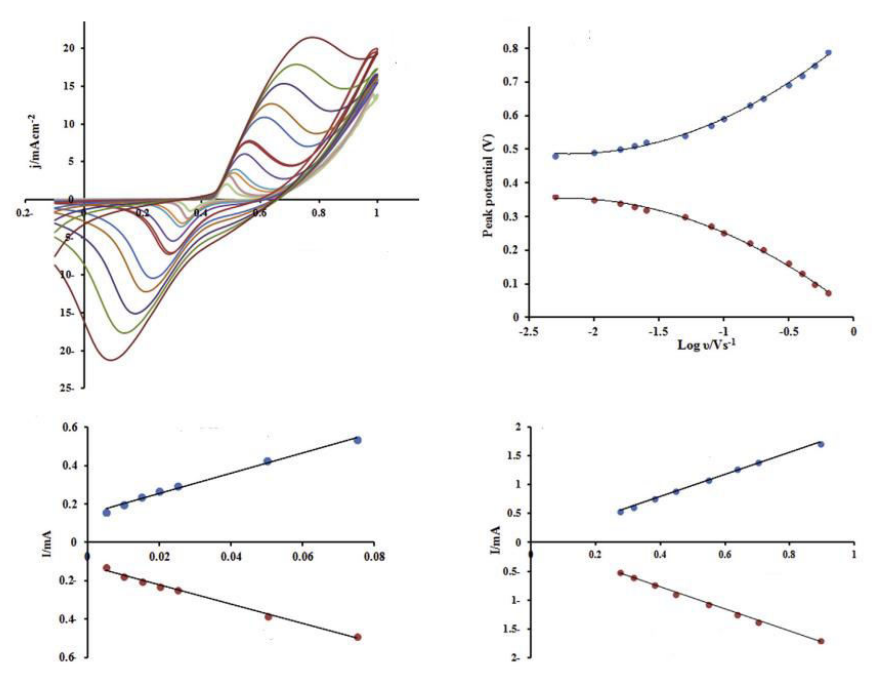


Figure 2. Cyclic voltammograms captured on the NiSBA-16CPE in 0.1 M NaOH at different scan speeds (A). (B) Cyclic voltammograms including anodic and cathodic peaks, with Ep shown against log n. (C) How Ipa and Ipc rely on n at lower values, and (D) depend on n1/2 at larger values and vice versa

Fig. 3a shows cyclic voltammograms of "CPE, NiCPE, SBA-16CPE, and NiSBA-16CPE" in a solution containing 0.03 MoleCH3OH in 0.1 Mole NaOH. This allowed us to trace the involvement of the modified electrode in the oxidation of CH3OH. Only on NiSBA-16CPE does the anodic oxidation rise current. Figure 3c and d show that the "mesoporous silica SBA-16 "does not have a major impact on the methanol oxidation process. NiSBA-16CPE has a significant number of holes, which increases the surface area for the absorption of Ni2+ ions. Figures 3a and b show that a tiny oxidation peak at 0.6 V, caused by the oxidation of methanol, was visible on the surface of NiCPE [30].

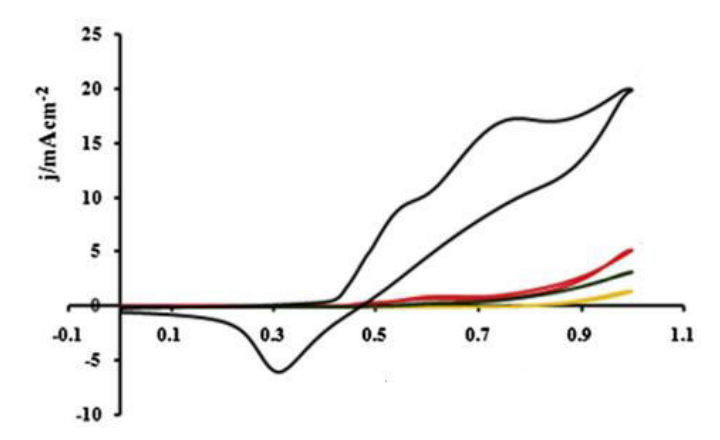


Figure 3. At a scan rate of 25 mV sL1, cyclic voltammograms were obtained on (a) CPE, (b) NiCPE, (c) SBA-16CPE, and (d) NiSBA-16CPE in the presence of 0.03 M methanol in 0.1 M NaOH

The electrocatalytic activity of the modified electrode is markedly affected by the NiSBA-16 ratio, with differences seen at 20%, 30%, and 40% loading levels. Experimental findings demonstrate that a 30% Ni(II) load on mesoporous SBA-16 nanoparticles yields the maximum anodic current for methanol oxidation, attributable to an ideal equilibrium between accessible catalytic sites and conductive routes. With an increase in nickel loading, the catalytic surface area for methanol oxidation expands, facilitating electron transport and augmenting methanol oxidation processes on the electrode surface. Nevertheless, owing to the intrinsically poor conductivity of SBA-16, augmenting the fraction of mesoporous silica above an ideal limit (30%) in the electrode may result in an increase in total resistance. This increased resistance presumably obstructs electron passage, hence reducing the efficiency of methanol oxidation. Moreover, an excess of SBA-16 in the matrix may dilute the active Ni(II) sites, hence diminishing the current density and eventually resulting in reduced electrocatalytic activity. This trade-off underscores the need of adjusting NiSBA-16 concentration in electrode design to attain both efficient charge transfer and strong catalytic activity.

3.2 NiSBA-16CPE conducts electrocatalytic oxidation of CH3OH.

Figure 4A shows the results of an analysis of the influence of CH3OH concentration on the cyclic voltammetry of "NiSBA-16CPE", which allowed us to analyze the electrochemical oxidation of CH3OH on the electrode surface. Two separate anodic peaks (p1 and p2) are seen at lower methanol concentrations, as shown in Figure 4B. Peak p1, which is about 0.56 Volt, is linked to the redox transition of the " α -Ni(OH)2/NiOOH" pair, while peak p2, at 0.78 Volt, is linked to the " β -Ni(OH)2/NiOOH" pair. Two distinct crystal structures of Ni(OH)2 are α -Ni(OH)2 and β -Ni(OH)2. As the electrochemical oxidation process with a Ni electrode progresses in an alkaline solution, the originally formed " α -Ni(OH)2 transforms into β -Ni(OH)2". The anodic sweep converts " α -Ni(OH)2 to β -Ni(OH)2" when methanol is present, and oxidation to NiOOH happens at peak p1 on NiSBA-16CPE. Peak p2 rises dramatically with increasing methanol concentration, but peak p1 decreases or vanishes altogether at these same concentrations. Despite the fact that " α -Ni(OH)2 oxidizes to NiOOH" at peak p1 in the anodic sweep, β -Ni(OH)2 is reduced to its original form when CH3OH is present. During the anodic scan, the current density at peak p2 grows in proportion to the concentration of methanol. This is because the oxidation process benefits from additional β -Ni(OH)2 active sites, which leads to the following catalytic process:

$$\beta - \text{Ni}(\text{OH})_2 + \text{OH}^- \rightarrow \text{Ni}(\text{OOH} + \text{H}_2\text{O} + \text{e}^- \dots 11$$

NiOOH + CH₃OH $\rightarrow \text{P}_{\text{OX}} + \text{Ni}(\text{OH})_2 \dots 12$

where Pox displays the byproducts of oxidizing methanol. Some of the possible byproducts of oxidizing methanol are carbonate, formaldehyde, and format. The process that Fleischmann et al. suggested yields RCOOH as a byproduct [31].

In the anodic direction, the peak currents of p1 and p2, which represent the "α -Ni(OH)₂/NiOOH and ϋ-Ni(OH)₂/NiOOH" redox couples, respectively, rise. In contrast, the cathodic sweep has a decreasing peak current associated with NiOOH reduction, and this decrease is strongly influenced by the concentration of methanol. A higher concentration of methanol during methanol oxidation allows for a larger conversion of NiOOH to η-Ni(OH)₂, leading to stronger anodic currents. On the other hand, as the concentration of methanol rises, the cathodic peak current drops because a-Ni(OH)₂ is formed during methanol oxidation, replacing available NiOOH active sites.

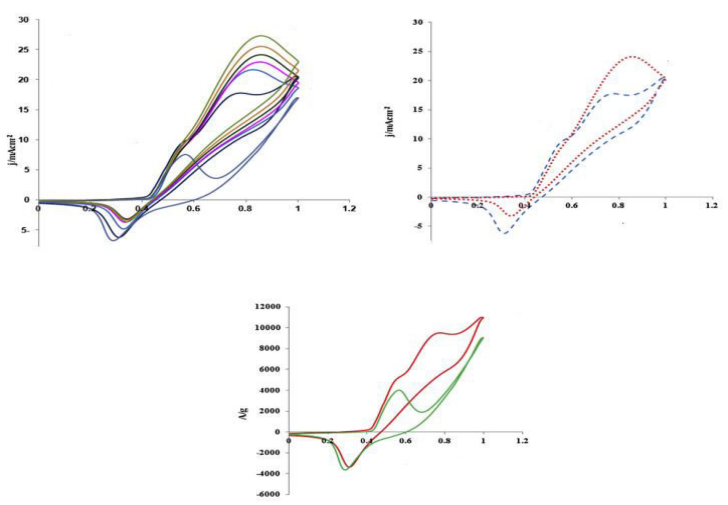


Figure 4. (A) NiSBA-16CPE current—potential curves for electrocatalytic methanol oxidation in a 0.1 M NaOH solution with varying methanol concentrations, scanned at a rate of 25 mV sL1.(B) From the main panel of (A), seen in the zoomed cyclic voltammograms of (b) and (e). (C) SBA-16CPE mass activity diagram

Reduction current drops off less sharply as the methanol concentration rises, as shown in Fig. 4. Based on the data, it seems that the reduction of nickel oxyhydroxide is a relatively sluggish response compared to its decrease.

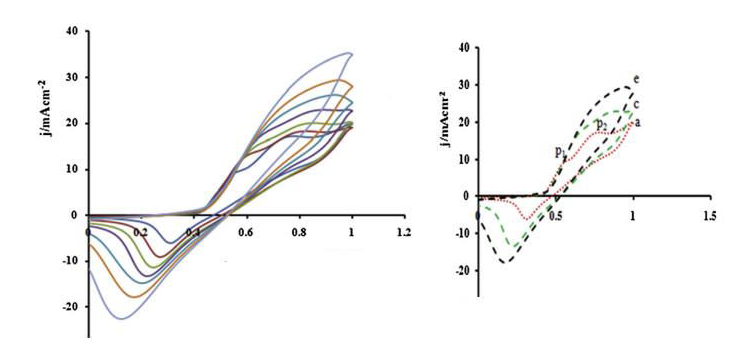


Figure 5.(A) NiSBA-16CPE cyclic voltammograms with 0.03 M methanol in 0.1 M NaOH, scan rates (B) Cyclic voltammograms zoomed

The cyclic voltammograms of NiSBA-16CPE acquired with 0.03 MoleCH3OH in 0.1 Mole NaOH are shown in Fig5. Rates of scan are between 25 and 300 mV s-1. Raising the san rates causes the anodic oxidation current to rise [32]. Figure 9B shows that there are two peaks, p1 and p2. Scan rate determines peak p2 height. When the scan rate is low (<0.15 V-1), peak p2 is visible; however, when the scan rate is large, it vanishes. According to these results, when the modified electrode is used, the e- transfer from active β -Ni(OH)₂/NiOOH to NiOOH is limited in space and time. When " α -Ni(OH)₂ is oxidized to NiOOH", the anodic current mostly forms

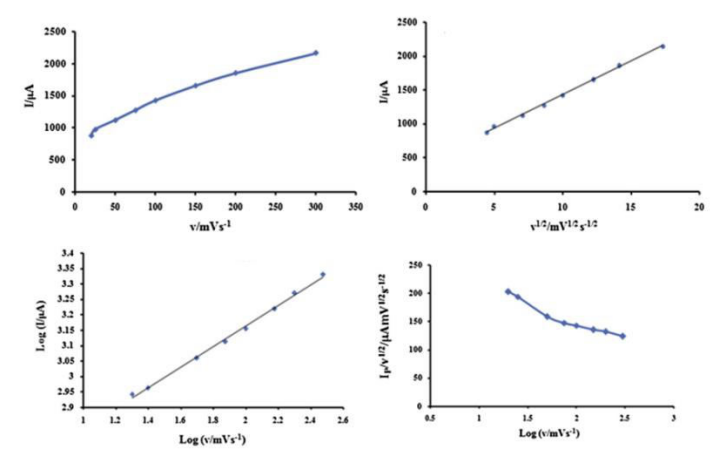


Figure 6. Plots of (a) Ipa vs. n (b) Ipa vs. n0.5 (c) Log Ipa vs. Log n (d) Ipa/n0.5 vs. log n for oxidation of 0.03 M methanol in 0.1 M NaOH at NiSBA-16CPE.

Figure 6a shows the Ipa versus n curve that was created by cyclic voltammetry of "NiSBA-16CPE in a solution that included 0.03 MoleCH3OH and 0.1 M NaOH". Figure 6b shows a plot of "peak current vs the square root of the scan rate", which suggests that the electrocatalytic process was regulated by diffusion rather than surface. A log Ipa against log v plot with an adsorption-controlled process should have a slope of 1.0 and a diffusion-controlled process should have a slope of 0.5, according to theory [33,34]. Figure 6c shows that during methanol oxidation on NiSBA-16CPE, there is a linear connection between log Ipa and log n. The slope of 0.33, which is calculated from the linear area, is very close to the theoretical value of 0.5, indicating that the current is mostly regulated by diffusion.

The modest discrepancy with theory, however, is due to the kinetic limitation's contribution to the process as a whole. Modified electrodes made of mesoporous materials, such SBA-16, are very stable even when exposed to high pH. The voltage was varied from 0 to 1 V. The solution began to absorb a trace amount of Ni²⁺ ions after many cycles. This is probably because Ni²⁺ binds strongly to SBA-16, which in turn binds to the mesoporous silica's pore walls. The result was that the adjusted electrode's peak current hardly changed [35]. Also, after three weeks, when 0.03 M methanol was present on the NiSBA-16CPE, the peak current density for methanol oxidation showed a slight drop in 0.1 M NaOH. Ni2+ leaking into solution or methanol oxidation product adsorption to NiOOH active sites are likely causes of the weakening of the anodic current. A range of methanol concentrations was also tested to determine NiSBA-16CPE's stability. A small reduction in the current density of the anodic oxidation current was seen after several sweep scan rates. When the methanol concentration is high, the current density drops significantly.

3.3 Chronoamperometric study

Chronoamperometry is used to measure the rate constant for CH3OH oxidation on the "NiSBA-16CPE" catalyst. The double-step chronoamperograms, or let curves, are shown in Figure 7. The first step involves establishing the modified electrode potential at 730 megavolts, and the second step is at 350 megavolt, with respect to Ag/AgCl. The Cottrell equation describes the observed diffusion-controlled mechanism, which is shown by the exponential amperograms.

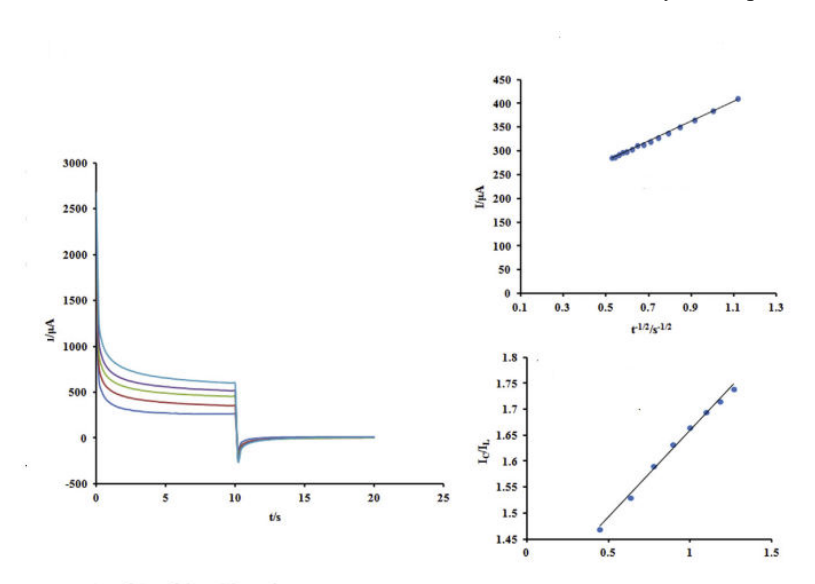


Figure 7.(A): dependence of current on t L1/2, derived from the data of chronoamperogram. (B): dependence of Ic/IL on t ½, derived from the data of chronoamperograms.

The following equation is used to compute the k of the electrocatalytic oxidation of CH3OH on the active sites of the "NiSBA-16CPE" modified electrode based on chronoamperograms [36]:

$$\frac{I_c}{I_L} = \gamma^{1/2} \left[\pi^{1/2} erf(\gamma^{1/2}) + exp(-\gamma) \gamma^{1/2} \right] \dots 16$$

The catalytic current of "NiSBA-16CPE" in the presence of CH3OH is denoted as Ic, the limiting current in the absence of CH3OH is denoted as IL, and the value of Υ is equal to kC0t, where C is the parameter of the error function. The reasoning uses the concentration of CH3OH in bulk solution, denoted as C0. Assuming Υ > 2, we see that Equation (16) is reduced to as the error function approaches 1:

$$\frac{I_c}{I_L} = \gamma^{1/2} \pi^{1/2} = \pi^{1/2} (k C_0 t)^{1/2} \dots 17$$

Co is the methanol concentration, t is the amount of time that has elapsed, and k is the catalytic rate constant. By analyzing the chronoamperogram of "NiSBA-16CPE" in both solutions with and without 0.1 MoleCH3OH in 0.1 MoleSodium hydroxide, one may determine the catalytic rate constant by calculating the slope of the linear plot of Ic/IL

vs. t 1/2. Equation (17) was used to find that the average value of k is about 1.184 x 103 per cubic centimeterper moleper second.

Conclusion

The electrocatalytic properties of Ni(II)-modified mesoporous silica in conjunction with carbon paste were examined by cyclic voltammetry and chronoamperometry. Cyclic voltammetry demonstrated an elevation in anodic oxidation current at the NiSBA-16CPE interface in methanol, but the cathodic current decreased. Modifying the electrode may mitigate the sluggish reaction rate in an alkaline solution by reducing the overpotential for methanol oxidation, thereby improving its efficiency. The lack of a peak in the anodic scan during studies with SBA-16CPE in methanol indicates that SBA-16 alone does not engage in the oxidation process. The electrocatalytic conversion of methanol necessitates Ni²⁺, which the non-conductive SBA-16 nanoparticles are incapable of supplying independently. Future research might investigate the incorporation of supplementary metal nanoparticles or conductive polymers into the SBA-16 framework to augment electron transport and boost the efficiency of methanol oxidation. The creation of novel hybrid materials with enhanced conductivity and catalytic characteristics may further reduce overpotentials. Furthermore, enhancing Ni(II) loading and adjusting the porosity of silica might improve overall electrocatalytic performance, presenting prospective uses in fuel cells and renewable energy systems.

References

- 1. Razmi H, Habibi E, Heidari H. Electrocatalytic oxidation of methanol and ethanol at carbon ceramic electrode modified with platinum nanoparticles. Electrochim Acta 2008;53:8178e85.
- 2. J. Aburto, M. Ayala, I. Bustos-Jaimes, C. Montiel, E. Terrés, J.M. Domínguez, E. Torres, Stability and catalytic properties of chloroperoxidase immobilized on SBA-16 mesoporous materials, Micropor. Mesopor. Mat. 83 (2005) 193–200.
- 3. Chen R, Congress SS, Cai G, Duan W, Liu S. Sustainable utilization of biomass waste-rice husk ash as a new solidified material of soil in geotechnical engineering: A review. Construction and Building Materials. 2021 Jul 19;292:123219.
- 4. Andrade GF, Soares DC, dos Santos RG, Sousa EM. Mesoporous silica SBA-16 nanoparticles: Synthesis, physicochemical characterization, release profile, and in vitro cytocompatibility studies. Microporous and mesoporous materials. 2013 Mar 1;168:102-10.
- 5. dos Santos SM, Nogueira KA, de Souza Gama M, Lima JD, da Silva Júnior IJ, de Azevedo DC. Synthesis and characterization of ordered mesoporous silica (SBA-15 and SBA-16) for adsorption of biomolecules. Microporous and Mesoporous Materials. 2013 Nov 1;180:284-92.
- 6. Lin DH, Jiang YX, Chen SR, Chen SP, Sun SG. Preparation of Pt nanoparticles supported on ordered mesoporous carbon FDU-15 for electrocatalytic oxidation of CO and methanol. Electrochimica acta. 2012 Apr 15;67:127-32.
- 7. Zhao D, Huo Q, Feng J, Chmelka BF, Stucky GD. Nonionic triblock and star diblock copolymer and oligomeric surfactant syntheses of highly ordered, hydrothermally stable, mesoporous silica structures. Journal of the American Chemical Society. 1998 Jun 24;120(24):6024-36.
- 8. Wang H, Wingender C, Baltruschat H, Lopez M, Reetz MT. Methanol oxidation on Pt, PtRu, and colloidal Pt electrocatalysts: a DEMS study of product formation. Journal of Electroanalytical Chemistry. 2001 Aug 24;509(2):163-9.
- 9. Naghiloo M, Yousefpour M, Nourbakhsh MS, Taherian Z. Functionalization of SBA-16 silica particles for ibuprofen delivery. Journal of Sol-Gel Science and Technology. 2015 May;74:537-43.
- 10. dos Santos SM, Nogueira KA, de Souza Gama M, Lima JD, da Silva Júnior IJ, de Azevedo DC. Synthesis and characterization of ordered mesoporous silica (SBA-15 and SBA-16) for adsorption of biomolecules. Microporous and Mesoporous Materials. 2013 Nov 1;180:284-92.
- 11. Mahmad-Toher AS, Govender N, Dorairaj D, Wong MY. Comparative evaluation on calcium silicate and rice husk ash amendment for silicon-based fertilization of Malaysian rice (Oryza sativa L.) varieties. Journal of Plant Nutrition. 2022 May 28;45(9):1336-47.
- 12. Naik B, Ghosh NN. A review on chemical methodologies for preparation of mesoporous silica and alumina based materials. Recent patents on nanotechnology. 2009 Nov 1;3(3):213-24.
- 13. Ho ST, Dinh QK, Tran TH, Nguyen HP, Nguyen TD. One-step synthesis of ordered Sn-substituted SBA-16 mesoporous materials using prepared silica source of rice husk and their selectively catalytic activity. The Canadian Journal of Chemical Engineering. 2013 Jan;91(1):34-46.
- 14. Que W, Hu X, Zhang QY. Preparation and optical properties of patternable TiO2/ormosils hybrid films for photonics applications. Chemical physics letters. 2003 Feb 17;369(3-4):354-60.
- 15. Thiedeitz M, Ostermaier B, Kränkel T. Rice husk ash as an additive in mortar–Contribution to microstructural, strength and durability performance. Resources, Conservation and Recycling. 2022 Sep 1;184:106389.
- 16. Bessel CA, Rolison DR. Topological redox isomers: surface chemistry of zeolite-encapsulated Co (salen) and [Fe (bpy) 3] 2+ complexes. The Journal of Physical Chemistry B. 1997 Feb 13;101(7):1148-57.
- 17. Jin Z, Liang H, Wang J. Temperature dependence in the synthesis of SBA-16-type mesoporous silica with pluronic F68 block copolymer. Journal of dispersion science and technology. 2010 Dec 21;32(1):28-34.

- 18. Xu W, Lo TY, Memon SA. Microstructure and reactivity of rich husk ash. Construction and Building Materials. 2012 Apr 1;29:541-7.
- 19. Ma J, Qiang L, Wang J, Tang D, Tang X. An easy route to synthesize novel mesostructured silicas Al/SBA-16 and its catalytic application. Catalysis letters. 2011 Feb;141:356-63.
- 20. Ma J, Qiang L, Wang J, Tang D, Tang X. An easy route to synthesize novel mesostructured silicas Al/SBA-16 and its catalytic application. Catalysis letters. 2011 Feb;141:356-63.
- 21. Tsoncheva T, Rosenholm J, Teixeira CV, Dimitrov M, Linden M, Minchev C. Preparation, characterization and catalytic behavior in methanol decomposition of nanosized iron oxide particles within large pore ordered mesoporous silicas. Microporous and Mesoporous Materials. 2006 Feb 24;89(1-3):209-18.
- 22. Shon JK, Kong SS, Kim YS, Lee J, Park WK, Park SC, et al. Microporous Mesoporous Mater 2009;120:441e6.
- 23. Marzouk HA, Arab MA, Fattouh MS, Hamouda AS. Effect of agricultural phragmites, rice straw, rice husk, and sugarcane bagasse ashes on the properties and microstructure of high-strength self-compacted self-curing concrete. Buildings. 2023 Sep 21;13(9):2394.
- 24. Kalapathy U, Proctor A, Shultz J. A simple method for production of pure silica from rice hull ash. Bioresource technology. 2000 Jul 1;73(3):257-62.
- 25. Bessel CA, Rolison DR. Topological redox isomers: surface chemistry of zeolite-encapsulated Co (salen) and [Fe (bpy)3] 2b complexes. J Phys Chem 1997;101:1148e57
- 26. Fleischmann M, Korinek K, Pletcher D. The oxidation of organic compounds at a nickel anode in alkaline solution. J Electroanal Chem 1971;31:39e49
- 27. Danaee I, Jafarian M, Forouzandeh F, Gobal F, Mahjani MG. Electrocatalytic oxidation of methanol on Ni and NiCu alloy modified glassy carbon electrode. Int J Hydrogen Energy 2008;33:4367e76
- 28. Laviron E. General expression of the linear potential sweep voltammogram in the case of diffusionless electrochemical systems. J Electroanal Chem 1979;101:19e28.
- 29. Taraszewska J, Roslonek G. Electrocatalytic oxidation of methanol on a glassy carbon electrode modified by nickel hydroxide formed by ex-situ chemical precipitation. J Electroanal Chem 1994;364:209e13.
- 30. Bard AJ, Faulkner LR. Electrochemical methods, fundamentals and applications. 2nd ed. New York: Wiley; 2001.
- 31. Zheng L, Song JF. Electrocatalytic oxidation of methanol and other short chain aliphatic alcohols at Ni(II)equercetin complex modified multi-wall carbon nano tube paste electrode. J Solid State Electrochem 2010;14:43e50.
- 32. Yi Q, Zhang J, Huang W, Liu X. Electrocatalytic oxidation of cyclohexanol on a nickel oxyhydroxide modified nickel electrode in alkaline solutions. J Catal Commun 2007;8:1017e22.
- 33. Subbaiah T, Mallick SC, Mishra KG, Sanjay K, Das RP. Electrochemical precipitation of nickel hydroxide. J Power Sources 2002;112:562e9.
- 34. Vela zquez-Palenzuela A, Centellas F, Antonio Garrido J, Arias C, Marı a Rodriguez R, Brillas E, et al. Kinetic analysis of carbon monoxide and methanol oxidation on high performance carbon-supported PteRu electrocatalyst for direct methanol fuel cells. J Power Sources 2011;196:3503e12.
- 35. Schön P, Krewer U. Revealing the complex sulfur reduction mechanism using cyclic voltammetry simulation. Electrochimica Acta. 2021 Mar 20;373:137523.
- 36. Coelho D, Luiz GM, Machado SA. Estimating the electrochemically active area: revisiting a basic concept in electrochemistry. Journal of the Brazilian Chemical Society. 2021 Oct 1;32(10):1912-7.